

Article

Simultaneous Characterization of Instantaneous Young's Modulus and Specific Membrane Capacitance of Single Cells Using a Microfluidic System

Yang Zhao ¹, Deyong Chen ¹, Yana Luo ¹, Feng Chen ¹, Xiaoting Zhao ², Mei Jiang ², Wentao Yue ², Rong Long ^{3,*}, Junbo Wang ^{1,*} and Jian Chen ^{1,*}

¹ State Key Laboratory of Transducer Technology, Institute of Electronics, Chinese Academy of Sciences, Beijing 100190, China; E-Mails: gaochunzy@gmail.com (Y.Z.); dychen@mail.ie.ac.cn (D.C.); luoyana88@126.com (Y.L.); ccmucf@aliyun.com (F.C.)

² Department of Cellular and Molecular Biology, Beijing Chest Hospital, Capital Medical University, Beijing 101149, China; E-Mails: zhao_xiaoting@126.com (X.Z.); jmcyf627@sina.com (M.J.); yuewentao@gmail.com (W.Y.)

³ Department of Mechanical Engineering, University of Alberta, Edmonton, AB T6G 2G8, Canada

* Authors to whom correspondence should be addressed; E-Mails: rlong2@ualberta.ca (R.L.); jbwang@mail.ie.ac.cn (J.W.); chenjian@mail.ie.ac.cn (J.C.); Tel.: +1-780-492-6534 (R.L.); +86-10-58887191 (J.W.); +86-10-58887531 (ext. 32-816) (J.C.); Fax: +1-780-492-2200 (R.L.); +86-10-58887191 (J.W.); +86-10-58887531 (ext. 32-816) (J.C.).

Academic Editor: Kwang W. Oh

Received: 6 December 2014 / Accepted: 19 January 2015 / Published: 27 January 2015

Abstract: This paper presents a microfluidics-based approach capable of continuously characterizing instantaneous Young's modulus ($E_{\text{instantaneous}}$) and specific membrane capacitance ($C_{\text{specific membrane}}$) of suspended single cells. In this method, cells were aspirated through a constriction channel while the cellular entry process into the constriction channel was recorded using a high speed camera and the impedance profiles at two frequencies (1 kHz and 100 kHz) were simultaneously measured by a lock-in amplifier. Numerical simulations were conducted to model cellular entry process into the constriction channel, focusing on two key parameters: instantaneous aspiration length ($L_{\text{instantaneous}}$) and transitional aspiration length ($L_{\text{transitional}}$), which was further translated to $E_{\text{instantaneous}}$. An equivalent distribution circuit model for a cell travelling in the constriction channel was used to determine $C_{\text{specific membrane}}$. A non-small-cell lung cancer cell line 95C ($n = 354$) was used to evaluate this technique, producing $E_{\text{instantaneous}}$ of 2.96 ± 0.40 kPa and $C_{\text{specific membrane}}$

of $1.59 \pm 0.28 \mu\text{F}/\text{cm}^2$. As a platform for continuous and simultaneous characterization of cellular $E_{\text{instantaneous}}$ and $C_{\text{specific membrane}}$, this approach can facilitate a more comprehensive understanding of cellular biophysical properties.

Keywords: microfluidics; single-cell analysis; cellular biophysics; instantaneous Young's modulus; specific membrane capacitance

1. Introduction

Mechanical properties of the cytoskeleton ($E_{\text{instantaneous}}$ and $E_{\text{equilibrium}}$) and electrical properties of cell membrane ($C_{\text{specific membrane}}$) determine the overall cellular biophysical properties [1] and have been correlated with diseases such as malaria and cancer [2,3]. Conventional techniques for cellular mechanical and/or electrical property characterization suffer from limited throughput and cannot quantify mechanical and electrical properties simultaneously [4,5] (e.g., ~20 cells per cell type based on electrorotation [6] and ~10 cells per cell type based on atomic force microscopy [7]).

Advances in microfluidic technologies have enabled mechanical and/or electrical property characterization of single cells in a continuous manner [8–11] (e.g., $E_{\text{instantaneous}}$ values from hundreds of A549 cells [12] and $C_{\text{specific membrane}}$ values from hundreds of H1299 cells [13,14]). However, the majority of reported microfluidic devices were only designed for characterizing either electrical or mechanical properties of a cell, but not both.

Previously, there are three types of devices developed to combine the measurements of cellular mechanical and electrical properties. These approaches were based on principles of microcantilever-based electrodes [15], micropipette aspiration with impedance spectroscopy [16], and constriction channel with impedance spectroscopy [17,18], respectively. Approaches using microcantilever-based electrodes [15] and the combination of micropipette aspiration with impedance spectroscopy [16] have limited throughput and cannot collect data from hundreds of single cells.

In [17,18], single cells were continuously aspirated through a constriction channel (a cross sectional area smaller than cells) while cellular images and single-frequency impedance profiles were obtained simultaneously and translated to cellular mechanical (cellular transition time through the constriction channel) and electrical (impedance amplitude increase during the cellular travelling process within the constriction channel) properties. Although this approach is featured with a higher throughput, which is capable of collecting biophysical data from hundreds of single cells, due to the lack of equivalent mechanical and electrical models, this method cannot interpret raw mechanical and electrical data into intrinsic cellular biophysical parameters ($E_{\text{instantaneous}}$ and $C_{\text{specific membrane}}$), leading to compromised capabilities in cell status evaluation and cell type classification [19].

Motivated by this challenge, in this paper, we present a constriction channel based microfluidic platform for simultaneous characterization of the intrinsic mechanical and electrical properties of single cells in a continuous manner (see Figure 1). In this platform, single cells were aspirated continuously through a constriction channel while the cellular entry process was imaged by a high speed camera and the two-frequency impedance profiles were measured by an impedance analyzer.

Based on equivalent mechanical and electrical models, these raw data were translated to $E_{\text{instantaneous}}$ and $C_{\text{specific membrane}}$, providing a comprehensive understanding of cellular biophysical properties.

Note that this platform is not a simple integration of previous constriction channel based microfluidic devices capable of characterizing either cellular instantaneous Young's modulus ($E_{\text{instantaneous}}$) [12] or specific membrane capacitance ($C_{\text{specific membrane}}$) [13,14]. The simultaneous collection of cellular images and two-frequency impedance data can provide more insights to study cellular behaviors during their entry and traveling processes within the constriction channel and thus provide a more complete characterization of biological cells.

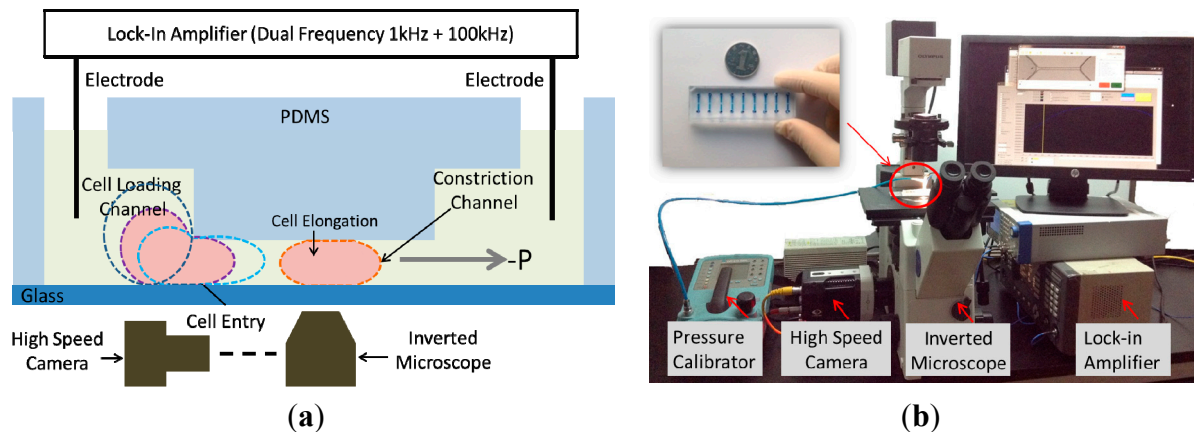


Figure 1. (a) Schematic and (b) setup of the microfluidic system for continuous characterization of $E_{\text{instantaneous}}$ and $C_{\text{specific membrane}}$ of single cells where cells are aspirated continuously through the constriction channel with cellular entry and traveling images as well as impedance profiles obtained simultaneously and translated to $E_{\text{instantaneous}}$ and $C_{\text{specific membrane}}$ based on proposed equivalent mechanical and electrical models.

2. Materials and Methods

2.1. Materials

All cell-culture reagents were purchased from Life Technologies Corporation (Carlsbad, CA, USA) unless otherwise specified. The materials used during device fabrication were SU-8 photoresist (MicroChem Corp., Newton, MA, USA) and 184 silicone elastomer (Dow Corning Corp., Midland, MI, USA). The non-small-cell lung cancer cell line 95C was cultured at 37 °C in 5% CO₂ in RPMI 1640 medium supplemented with 10% heat-inactivated fetal bovine serum, 100 units/mL penicillin and 100 µg/mL streptomycin.

2.2. Device Fabrication and Operation

The microfluidic device consists of a constriction channel (cross-section area: 10 µm × 10 µm) in polydimethylsiloxane (PDMS) elastomer that was replicated from a double-layer SU-8 mold. The detailed fabrication procedures were described in a previous publication [20]. Briefly, SU-8 5 was spin coated and exposed without development to form the constriction channel with a height of 10 µm. Then SU-8 25 (cell loading channel with a height of 25 µm) was spin coated on top of the first SU-8

layer, exposed with alignment and developed, forming the two-layer mold master. PDMS prepolymers and curing agents (10:1 in weight) were mixed, poured on channel masters and baked in an oven for crosslinking. PDMS channels were then peeled from the SU-8 masters, punched to form reservoir holes, and bonded to glass slides after plasma treatment.

During operation the device was first filled with culture medium and a droplet of cell suspension (1×10^6 cells/mL) was pipetted onto the entrance of the cell loading channel. A negative pressure of 500 Pa generated from a pressure calibrator (DPI-610 pressure calibrator, Druck, Billerica, MA, USA) was applied to aspirate cells continuously through the constriction channel while silver electrode wires [16] were inserted into the inlet and the outlet of the PDMS device for impedance profile monitoring. Cell images were taken by an inverted microscope (IX71, Olympus Inc., Tokyo, Japan) connected with a Phantom M320S high speed camera (Phantom Inc., Bublin, OH, USA) at 200 frames per second. Two-frequency impedance data (1 kHz + 100 kHz) was sampled by a Model 7270 DSP lock-in amplifier (Signal Recovery, Oak Ridge, TN, USA) with a sampling rate of 20 points per second. Note that impedance data at 1 kHz were used to evaluate the sealing properties of deformed cells with constriction channel walls and impedance data at 100 kHz were used to quantify equivalent cellular membrane capacitance and cytoplasm resistance. All the characterization experiments were conducted within 30 min after cell trypsinization.

2.3. Equivalent Mechanical and Electrical Models

Numerical simulations were performed using a finite element package ABAQUS (version 6.11, Dassault Systemes Simulia Corp., Providence, RI, USA) to model cellular entry process into the constriction channel with detailed procedures described in a previous publication [12]. Briefly, the channel walls were modeled as rigid surfaces with a geometrical parameter of $D_{channel}$ and the cell was modeled as an incompressible solid with a key mechanical parameter of $E_{instantaneous}$. The friction on cell-wall interface was modeled with a constant friction coefficient f_c .

Figure 2a–d show the simulation results of the cellular entry process including the stage I of instantaneous jump into the channel ($L_{instantaneous}$) (see Figure 2a) and the stage II of cellular creep response (Figure 2b,c), with the ending point at the transitional position ($L_{transitional}$) (Figure 2d). Numerical simulation shows that $L_{instantaneous}/D_{channel}$ and $L_{transitional}/D_{channel}$ are functions of two variables $P_{aspiration}/E_{instantaneous}$ (linear function) and f_c as follows ($P_{aspiration}$ represents aspiration pressure applied to aspirate cells into the constriction channel) [12]:

$$L_{instantaneous}/D_{channel} = (44.27f_c^2 - 37.24f_c + 13.70) \times P_{aspiration}/E_{instantaneous} - 5.31f_c^2 + 2.84f_c - 0.59$$

$$L_{transitional}/D_{channel} = (-60.40f_c^2 + 40.05f_c - 8.68) \times P_{aspiration}/E_{instantaneous} + 1.99f_c^2 + 0.03f_c + 1.60$$

An equivalent circuit model (see Figure 2e) was proposed to model the cellular traveling process within the constriction channel with detailed description shown in a previous publication [13]. Briefly, distributed leakage resistors were represented by $R_{L1}, R_{L2}, \dots, R_{Ln}, R_{Ln+1}$ with n divisions ($n \geq 2$) along the cell elongation direction while cellular electrical components were represented by $C_{Ms}, C_{Mp1}, \dots, C_{Mpn}$ and R_{C1}, \dots, R_{Cn+1} , respectively. These distributed equivalent membrane capacitors can be further represented by $C_{specific\ membrane}$ as follows ($L_{cell\ elongation}$ represents the length of an elongated biological cell travelling within the constriction channel) [13]:

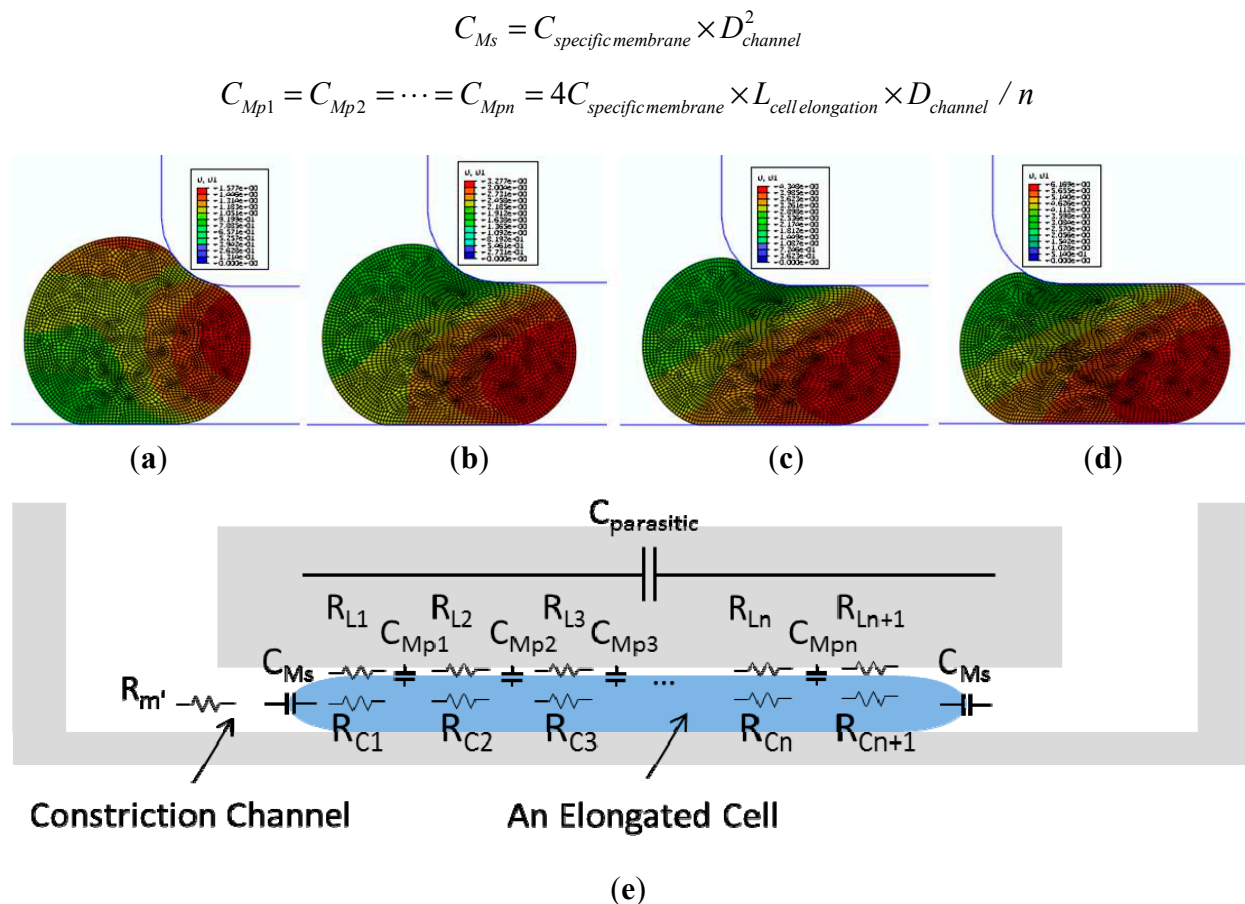


Figure 2. (a–d) Numerical simulations to model the cellular entry process including (a) initial jump into the channel; (b,c) cellular creep response and (d) creep response termination at the transitional position; (e) The proposed equivalent circuit model for a travelling cell within the constriction channel where C_{Ms} , C_{Mp1} , ..., C_{Mpn} and R_{C1} , ..., R_{Cn+1} represent distributed membrane capacitance and cytoplasm resistance with n divisions along the cell elongation direction. Note that R_{L1} , R_{L2} , ..., R_{Ln} , R_{Ln+1} represent distributed leakage resistors, indicating the sealing properties of deformed cells with constriction channel walls.

2.4. Data Analysis

To measure the elongation length of a cell while it is travelling in the constriction channel, we used a previously developed background subtraction technique to process the images captured by the high-speed camera. This technique consists of a sequence of image processing steps adapted to the context of cell elongation (frame differencing, thresholding, particle removal using erosion, and edge detection along the channel) [21].

Based on the equivalent mechanical model in Section 2.3, raw data of cellular aspiration length were translated to intrinsic cellular mechanical parameter of $E_{instantaneous}$ and based on the equivalent electrical model in Section 2.3, raw data of two-frequency impedance values and cell elongation length during its travelling inside the constriction channel were translated to intrinsic cellular electrical parameter of $C_{specific\ membrane}$.

3. Results and Discussion

Figure 3a–d show microscopic pictures of a typical 95C cell's entry process into the constriction channel with raw impedance data of the same cell recorded at 1 kHz and 100 kHz (Figure 3e). Based on the quantified aspiration length (the distance between the leading tip of the cell and the beginning of the constriction channel) vs. time (see Figure 3f), the cellular entry process was divided into two stages.

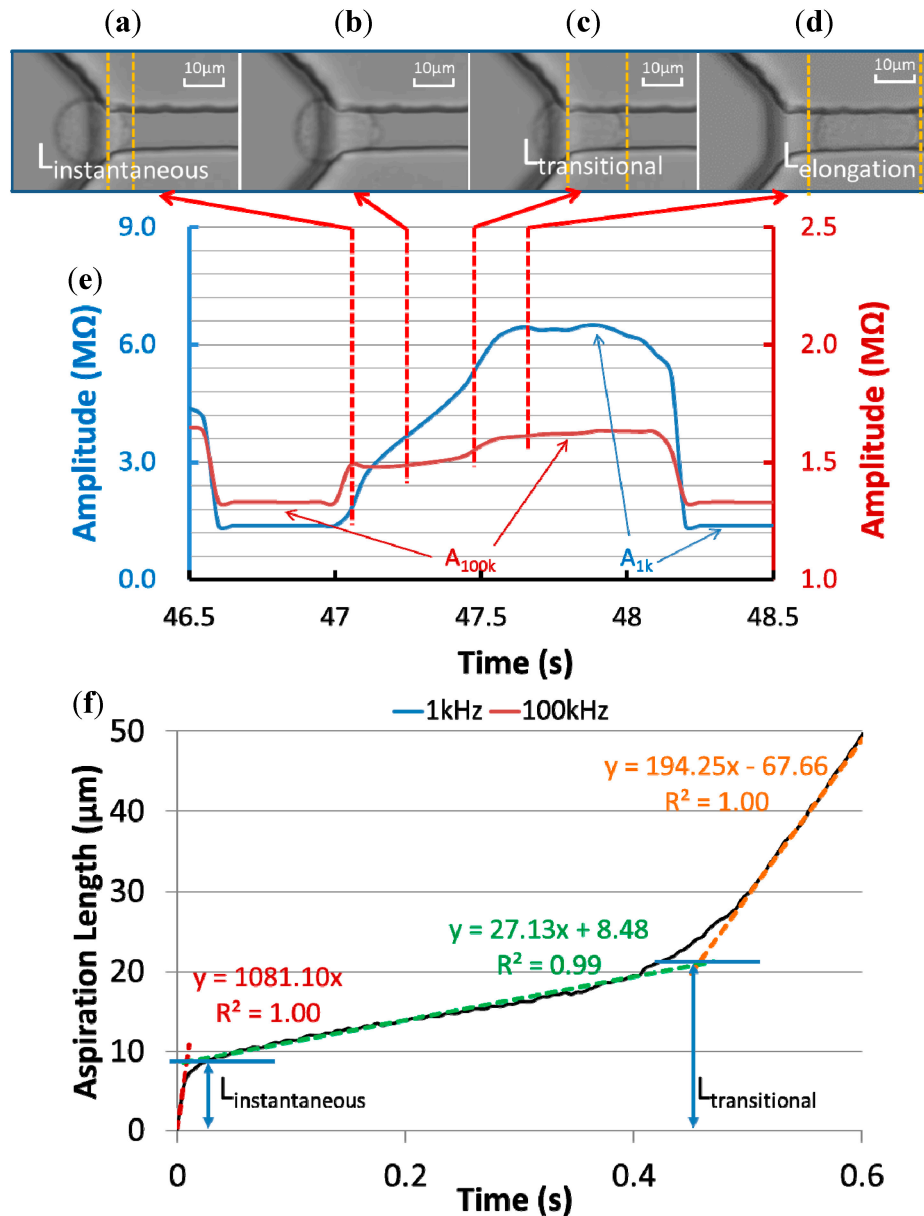


Figure 3. (a–d) Microscopic pictures of a 95C cell's entry process into the constriction channel with raw impedance data of the same cell shown in (e) and aspiration length vs. time shown in (f). Based on raw data processing, four critical parameters $L_{\text{instantaneous}}$, $L_{\text{transitional}}$, $A_{1\text{ kHz}}$ and $A_{100\text{ kHz}}$ were obtained.

In stage I, an instantaneous jump into the constriction channel was observed (see Figure 3a), characterized by the instantaneous aspiration length ($L_{\text{instantaneous}}$) in Figure 3f. An instantaneous amplitude jump at 100 kHz and the initiation of a gradual amplitude increase at 1 kHz were also found

in this stage. The 100 kHz electric lines were used to penetrate capacitive cellular membrane portions and in stage I its instantaneous increase in amplitude indicates the existence of an equivalent capacitor representing the leading membrane portion, which was sucked into the constriction channel instantly. The 1 kHz electric lines were used to pass around capacitive cellular membrane portions and in stage I, due to the limited aspiration length of the cell under measurement, no significant increase in amplitude at 1 kHz was observed.

After the instantaneous jump, a gradual increase in aspiration length (see Figure 3b,f) was observed due to the cellular creeping behaviour, and this was defined as stage II. During this stage, there is a gradual increase in amplitude at 1 kHz, confirming a gradual increase of the cellular aspiration length. On the other hand, no significant increase in amplitude at 100 kHz was observed, which is due to the fact that the area of the membrane portion sucked into the constriction channel was much smaller than the membrane portion left outside of the constriction channel and thus the contribution of the equivalent capacitor for the portion outside of the constriction channel was negligible.

With further increase in aspiration length while the cell continues to deform due to viscoelastic relaxation, a transitional position quantified as transitional aspiration length ($L_{transitional}$) was reached (see Figure 3c), which is the end of the creep stage and the cell rapidly enters the channel. From the perspective of impedance measurement, there is a slope (amplitude/time) increase at 1 kHz, confirming the initiation of accelerated cellular entry into the constriction channel.

In addition, a gradual increase in the impedance amplitude at 100 kHz was noticed for this transition status since as the cell started to enter the constriction channel rapidly, both membrane portions for the leading edge and the trailing edge make contribution to the impedance profiles at 100 kHz.

Figure 3d shows the microscopic picture of the cell travelling within the constriction channel and at this stage, stable impedance amplitudes at 1 kHz and 100 kHz were observed. Furthermore, two critical parameters $A_{1\text{ kHz}}$ (the amplitude ratio between the stable impedance amplitude at 1 kHz with travelling cells to the basal impedance amplitude at 1 kHz without cells) and $A_{100\text{ kHz}}$ (the amplitude ratio between the stable impedance amplitude at 100 kHz with travelling cells to the basal impedance amplitude at 100 kHz without cells) were calculated for cellular electrical property quantification.

Figure 4a,b show scatter plots of cellular mechanical data of $L_{instantaneous}/D_{channel}$ vs. D_{cell} (a) and $L_{transitional}/D_{channel}$ vs. D_{cell} (b), respectively, for 95C cells ($n = 354$). Quantified $L_{instantaneous}/D_{channel}$ and $L_{transitional}/D_{channel}$ were 0.76 ± 0.15 and 2.00 ± 0.40 where $D_{channel}$ represents the characteristic channel dimension (10 μm). It was noticed that with an increase in cell diameter, there is a corresponding increase for $L_{transitional}/D_{channel}$ where $L_{instantaneous}/D_{channel}$ is not dependent on D_{cell} . This observation was consistent with the previous study where $E_{instantaneous}$ played a major role in determining $L_{instantaneous}/D_{channel}$ while $L_{transitional}/D_{channel}$ is mainly determined by f_c and D_{cell} [12].

Figure 4c,d show scatter plots of cellular electrical data of $A_{1\text{ kHz}}$ vs. $L_{cell\text{ elongation}}$ (c) and $A_{100\text{ kHz}}$ vs. $L_{cell\text{ elongation}}$ (d), respectively, for 95C cells ($n = 354$). Quantified $A_{1\text{ kHz}}$ and $A_{100\text{ kHz}}$ were 3.92 ± 1.09 and 1.29 ± 0.04 where $L_{cell\text{ elongation}}$ represents the cellular elongation length during its travelling process within the constriction channel as an indicator of cell sizes. Compared to $A_{1\text{ kHz}}$, $A_{100\text{ kHz}}$ was significantly lower since electric lines at 100 kHz effectively penetrate the cellular membrane portions while electric lines at 1 kHz always travel around capacitive cellular membrane portions. With the increase in $L_{cell\text{ elongation}}$, a corresponding increase in $A_{1\text{ kHz}}$ was observed, further confirming the assumption that electric lines at 1 kHz pass around cells rather than penetrate cellular membrane portions.

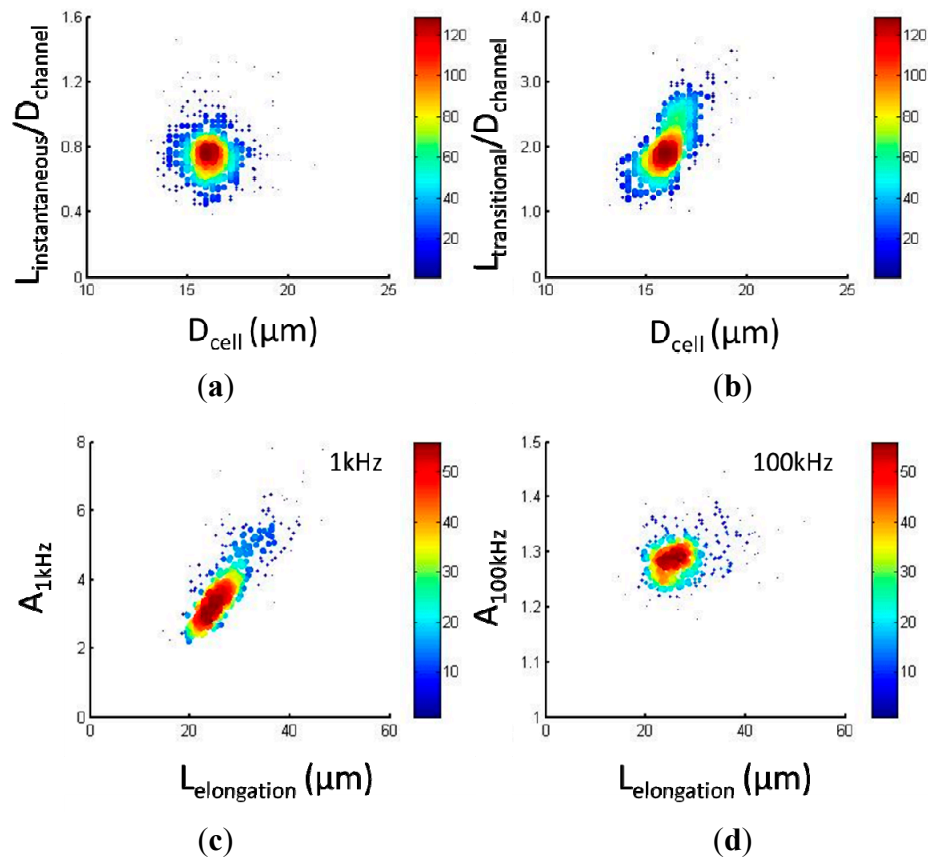


Figure 4. (a–d) Scatter plots of raw mechanical data of $L_{\text{instantaneous}}/D_{\text{channel}}$ vs. D_{cell} (a) and $L_{\text{transitional}}/D_{\text{channel}}$ vs. D_{cell} (b) as well as raw electrical data of $A_{1\text{kHz}}$ vs. $L_{\text{cell elongation}}$ (c) and $A_{100\text{kHz}}$ vs. $L_{\text{cell elongation}}$ (d) for 95C cells ($n = 354$).

Figure 5a shows the scatter plot of $C_{\text{specific membrane}}$ vs. $E_{\text{instantaneous}}$, which were quantified as 2.96 ± 0.40 kPa ($E_{\text{instantaneous}}$) vs. 1.59 ± 0.28 $\mu\text{F}/\text{cm}^2$ ($C_{\text{specific membrane}}$) for 95C cells ($n = 354$) (see Figure 5b). Figure 5c,d shows distribution percentages of $E_{\text{instantaneous}}$ and $C_{\text{specific membrane}}$ for 95C cells with the peak of $E_{\text{instantaneous}}$ within the range of 2.6–2.9 kPa and $C_{\text{specific membrane}}$ within the range of 1.4–1.6 $\mu\text{F}/\text{cm}^2$. These reported values were consistent with previously reported values [12,14], confirming that the proposed microfluidic platform is capable of characterizing cellular intrinsic mechanical and electrical markers simultaneously.

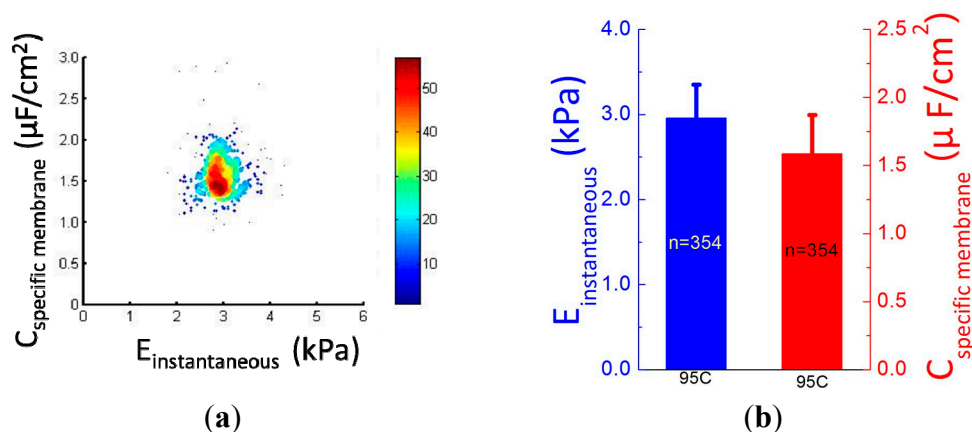


Figure 5. Cont.

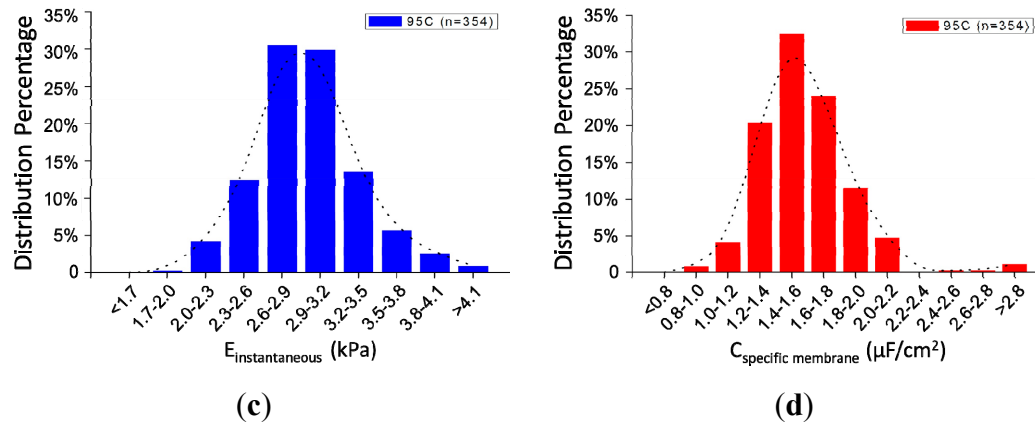


Figure 5. (a) A scatter plot of $C_{\text{specific membrane}}$ vs. $E_{\text{instantaneous}}$ for 95C cells ($n = 354$) with quantified $E_{\text{instantaneous}}$ of 2.96 ± 0.40 kPa and $C_{\text{specific membrane}}$ of 1.59 ± 0.28 $\mu\text{F}/\text{cm}^2$ shown in (b). (c) and (d) Distribution percentages of $E_{\text{instantaneous}}$ and $C_{\text{specific membrane}}$ for 95C cells with the peak of $E_{\text{instantaneous}}$ within the range of 2.6–2.9 kPa and $C_{\text{specific membrane}}$ within the range of 1.4–1.6 $\mu\text{F}/\text{cm}^2$.

4. Conclusions

This paper presented a microfluidic measurement system for characterizing $E_{\text{instantaneous}}$ and $C_{\text{specific membrane}}$ of single cells using constriction channel and impedance spectroscopy. Both microscopic images and impedance profiles confirmed the two-stage cellular entry process into the constriction channel, enabling the quantification of $L_{\text{instantaneous}}$ and $L_{\text{transitional}}$ as key mechanical parameters, which were then translated to $E_{\text{instantaneous}}$. Furthermore, based on the distributed equivalent circuit model for cellular travelling within the constriction channel, impedance profiles at two frequencies were obtained and translated to $C_{\text{specific membrane}}$. Compared to previous approaches, this technique is capable of characterizing both $E_{\text{instantaneous}}$ and $C_{\text{specific membrane}}$ in a continuous manner, which can potentially lead to a more complete understanding of cellular biophysical properties.

Acknowledgments

The authors would like to acknowledge financial support from National Natural Science Foundation of China (Grant No. 61201077), National Basic Research Program of China (973 Program, Grant No. 2014CB744600), National Natural Science Foundation of China (Grant No. 81261120561 and No. 61431019), National High Technology Research and Development Program of China (863 Program, Grant No. 2014AA093408), Instrument Development Program of Chinese Academy of Sciences (2015–2016) and Beijing NOVA Program.

Author Contributions

Y.Z., Y.L. and X.Z. designed and conducted experiments; F.C. and W.Y. analyzed the data; D.C. and R.L. contributed to equivalent electrical and mechanical models; M.J. conducted cell culture; J.W. and J.C. organized the experiments and drafted the paper.

Conflicts of Interest

The authors declare no conflict of interest.

References

1. Ethier, C.R.; Simmons, C.A. *Introductory Biomechanics: From Cells to Organisms*; Cambridge University Press: Cambridge, UK, 2007.
2. Lee, G.Y.H.; Lim, C.T. Biomechanics approaches to studying human diseases. *Trends Biotechnol.* **2007**, *25*, 111–118.
3. Suresh, S. Biomechanics and biophysics of cancer cells. *Acta Biomater.* **2007**, *3*, 413–438.
4. Kim, D.H.; Wong, P.K.; Park, J.; Levchenko, A.; Sun, Y. Microengineered platforms for cell mechanobiology. *Ann. Rev. Biomed. Eng.* **2009**, *11*, 203–233.
5. Valero, A.; Braschler, T.; Renaud, P. A unified approach to dielectric single cell analysis: Impedance and dielectrophoretic force spectroscopy. *Lab Chip* **2010**, *10*, 2216–2225.
6. Becker, F.F.; Wang, X.B.; Huang, Y.; Pethig, R.; Vykoukal, J.; Gascoyne, P.R.C. Separation of human breast-cancer cells from blood by differential dielectric affinity. *Proc. Natl. Acad. Sci. USA* **1995**, *92*, 860–864.
7. Cross, S.E.; Jin, Y.S.; Rao, J.; Gimzewski, J.K. Nanomechanical analysis of cells from cancer patients. *Nat. Nanotechnol.* **2007**, *2*, 780–783.
8. Mao, X.; Huang, T.J. Exploiting mechanical biomarkers in microfluidics. *Lab Chip* **2012**, *12*, 4006–4009.
9. Zheng, Y.; Sun, Y. Microfluidic devices for mechanical characterisation of single cells in suspension. *Micro Nano Lett.* **2011**, *6*, 327–331.
10. Cheung, K.C.; di Berardino, M.; Schade-Kampmann, G.; Hebeisen, M.; Pierzchalski, A.; Bocsi, J.; Mittag, A.; Tárnok, A. Microfluidic impedance-based flow cytometry. *Cytometry A.* **2010**, *77*, 648–666.
11. Yobas, L. Microsystems for cell-based electrophysiology. *J. Micromech. Microeng.* **2013**, *23*, 083002.
12. Luo, Y.; Chen, D.; Zhao, Y.; Wei, C.; Zhao, X.; Yue, W.; Long, R.; Wang, J.B.; Chen, J. A constriction channel based microfluidic system enabling continuous characterization of cellular instantaneous Young's modulus. *Sens. Actuators B Chem.* **2014**, *202*, 1183–1189.
13. Zhao, Y.; Chen, D.; Luo, Y.; Li, H.; Deng, B.; Huang, S.-B.; Chiu, T.-K.; Wu, M.-H.; Long, R.; Hu, H.; *et al.* A microfluidic system for cell type classification based on cellular size-independent electrical properties. *Lab Chip* **2013**, *13*, 2272–2277.
14. Zhao, Y.; Zhao, X.T.; Chen, D.Y.; Luo, Y.N.; Jiang, M.; Wei, C.; Long, R.; Yue, W.T.; Wang, J.B.; Chen, J. Tumor cell characterization and classification based on cellular specific membrane capacitance and cytoplasm conductivity. *Biosens. Bioelectron.* **2014**, *57*, 245–253.
15. Cho, Y.H.; Yamamoto, T.; Sakai, Y.; Fujii, T.; Kim, B. Development of microfluidic device for electrical/physical characterization of single cell. *J. Microelectromech. Syst.* **2006**, *15*, 287–295.

16. Chen, J.; Zheng, Y.; Tan, Q.; Zhang, Y.L.; Li, J.; Geddie, W.R.; Jewett, M.A.S.; Sun, Y. A microfluidic device for simultaneous electrical and mechanical measurements on single cells. *Biomicrofluidics* **2011**, *5*, 14113.
17. Chen, J.; Zheng, Y.; Tan, Q.; Shojaei-Baghini, E.; Zhang, Y.L.; Li, J.; Prasad, P.; You, L.; Wu, X.Y.; Sun, Y. Classification of cell types using a microfluidic device for mechanical and electrical measurement on single cells. *Lab Chip* **2011**, *11*, 3174–3181.
18. Zheng, Y.; Shojaei-Baghini, E.; Azad, A.; Wang, C.; Sun, Y. High-throughput biophysical measurement of human red blood cells. *Lab Chip* **2012**, *12*, 2560–2567.
19. Zheng, Y.; Nguyen, J.; Wei, Y.; Sun, Y. Recent advances in microfluidic techniques for single-cell biophysical characterization. *Lab Chip* **2013**, *13*, 2464–2483.
20. Zhao, Y.; Chen, D.; Li, H.; Luo, Y.; Deng, B.; Huang, S.B.; Chiu, T.-K.; Wu, M.-H.; Long, R.; Hu, H.; *et al.* A microfluidic system enabling continuous characterization of specific membrane capacitance and cytoplasm conductivity of single cells in suspension. *Biosens. Bioelectron.* **2013**, *43C*, 304–307.
21. Huang, S.B.; Zhao, Z.; Chen, D.Y.; Lee, H.C.; Luo, Y.N.; Chiu, T.K.; Wang, J.; Chen, J.; Wu, M.-H. A clogging-free microfluidic platform with an incorporated pneumatically-driven membrane-based active valve enabling specific membrane capacitance and cytoplasm conductivity characterization of single cells. *Sens. Actuators B Chem.* **2014**, *190*, 928–936.

© 2015 by the authors; licensee MDPI, Basel, Switzerland. This article is an open access article distributed under the terms and conditions of the Creative Commons Attribution license (<http://creativecommons.org/licenses/by/4.0/>).